

Chapter 3

Spatially resolved spectroscopy of Titan

3.1 Introduction

While the Voyager 1 flyby of Titan in 1980 established the structure and composition of Titan's atmosphere (Lindal *et al.*, 1983), little could be distinguished below a thick layer of haze which fills the stratosphere. The haze is the end-product of the photolysis of N_2 and CH_4 , the two most common atmospheric constituents (Kunde *et al.*, 1981; Yung *et al.*, 1984). Although the main haze layer was optically thick to Voyager's visible-light cameras, some structure was clearly apparent in its uppermost regions, such as a detached global haze layer at 300–350 km altitude, a north polar hood, and a pronounced hemispheric albedo contrast (Smith *et al.*, 1981; Rages and Pollack, 1983). The hemispheric brightness asymmetry appears to alternate seasonally (Caldwell *et al.*, 1992; Lorenz *et al.*, 1997, 1999, 2001), consistent with transport of haze across Titan's equator by thermally direct winds (Sromovsky *et al.*, 1981; Hutzell *et al.*, 1996). Thus it appears that Titan's haze distribution is shaped by both the latitude-dependent environment of the stratosphere, and by dynamical transport of aerosols. An important recent advance in understanding the haze distribution has been the coupling of a microphysical haze production model (McKay *et al.*, 2001) with a global circulation model which takes into account the radiative properties of the haze, which together reproduce many of these observed features (Rannou *et al.*, 2002).

Observations through near-infrared spectral windows in Titan's atmosphere have now revealed a complex surface (Smith *et al.*, 1996; Combes *et al.*, 1997; Gibbard *et al.*, 1999; Meier *et al.*, 2000; Coustenis *et al.*, 2001) and transient CH_4 clouds near Titan's south pole

(Griffith *et al.*, 1998, 2000; Brown *et al.*, 2002; Roe *et al.*, 2002), yet the distribution of haze and long-lived clouds in the troposphere is poorly constrained. Titan’s surface must provide the ultimate sink for the haze, but it is unclear whether condensation of CH₄ on the aerosols once below the tropopause (at 40 km altitude) might increase their fall velocity and clear out the region, or whether condensation is inhibited for kinetic or chemical compatibility reasons (McKay, 1996; Samuelson and Mayo, 1997; Samuelson *et al.*, 1997). If rain-out of the haze does occur, it is possible that the CH₄ would re-evaporate before reaching the surface, leaving a separate low aerosol layer (Lorenz, 1993).

Two recent observational studies have attempted to map the distribution of haze and clouds in Titan’s lower stratosphere and troposphere. Young *et al.* (2002) analyzed narrow-band 890–950 nm Hubble Space Telescope (HST) images, using the strongly varying CH₄ absorption over this spectral region to constrain the altitude structure of the haze in the lower stratosphere and troposphere. They find an apparent gap in the haze at 16–32 km altitude, underlain by an optically thick region between the surface and 16 km. However, the apparent presence of this lower haze layer is likely to be a consequence of their assumption of a zero-albedo surface, since its claimed thickness correlates closely with the actual surface albedo distribution (Fig. 6.5). Chanover *et al.* (2003) provide further evidence for a relatively clear atmosphere below 30–60 km altitude in Titan’s equatorial region.

Understanding the vertical distribution of haze and other condensates in Titan’s lower atmosphere provides insight into the seasonally varying circulation patterns, and proves critical to correctly interpreting near-infrared images of Titan’s surface (Ch. 6). We present in this chapter the first spatially resolved near-infrared spectra of Titan’s atmosphere and surface, acquired with the Palomar Hale telescope adaptive optics (AO) system and PHARO spectrograph between September 1999 and December 2001. Spatially resolving Titan’s disk provides spectra of each latitude at a variety of emission angles, from which we determine both the vertical distribution of aerosols and condensates, and the underlying surface albedo. Though the spatial resolution of these data is not sufficient to resolve the small transient clouds recently discovered near Titan’s south pole (Brown *et al.*, 2002; Roe *et al.*, 2002), a broad region of high clouds is noted at high southern latitudes.

Sections 3.2 and 3.3 present in detail our observing strategy and the steps required to process and calibrate AO-corrected spectra, with the goal of providing a useful resource for future users of the Palomar AO system. Section 3.4 describes our analysis of these

spectra, by which we determine the three-dimensional haze and cloud structure of Titan’s atmosphere and the surface albedo distribution, presented in Section 3.5. Finally, Sec. 3.6 discusses the implications for Titan’s global atmospheric circulation, the physical conditions in the troposphere, and Titan’s surface composition.

3.2 Observations

Spectra of Titan were obtained on 26 September 1999, 20 July 2000, and 20 December 2001 UT using the JPL AO system and the Cornell-built PHARO camera/spectrograph at the Cassegrain focus of the Hale 5-m telescope. The AO system consists of a Shack-Hartmann sensor ($\lambda < 1.05 \mu\text{m}$) controlling a fast tip-tilt mirror and a 241-active element deformable mirror, which together partially correct atmosphere-induced wavefront aberrations of the $\lambda > 1.05 \mu\text{m}$ science beam (Dekany, 1996). Titan itself ($V \approx 8.2$) provided the reference source for these observations, allowing the deformable mirror to be run at a closed-loop servo bandwidth of ~ 20 Hz (500 Hz update rate). The PHARO near-infrared camera (Hayward *et al.*, 2001) was used to record both broad-band images and medium-resolution spectra of Titan. Images were taken through either a K-prime (K' , 1.945–2.296 μm) or K-short (K_s , 1.990–2.300 μm) filter, and recorded with the 1024×1024 pixel Rockwell HAWAII HgCdTe array detector at a platescale of $0''.0252 \text{ pix}^{-1}$ (Metchev *et al.*, 2003). To acquire AO-corrected spectra, an $0''.13 \times 40''$ slit was placed in the focal plane near the entrance to the PHARO camera, and a grism used to disperse the beam onto the same detector at a spectral resolution of $\lambda/\Delta\lambda = 1800$ over the wavelength range 2.03–2.37 μm , at a spatial platescale of $0''.040 \text{ pix}^{-1}$. The 20 July 2000 and 20 December 2001 observations recorded only the wavelength range 2.10–2.32 μm , due to a mistaken choice of the $0''.0252 \text{ pix}^{-1}$ platescale mode of the instrument.

The observing sequence was dictated by the need to reconstruct the pointing of each spectrum after the fact, and to maintain the spectral stability of PHARO throughout the observations. Before each set of Titan spectra, 4 to 16 dithered K' or K_s images of Titan with an integration time of 9.1 s were first acquired. These were used to estimate the point spread function (PSF) and the pointing of the subsequent spectra.

Since PHARO does not provide a slit-viewing capability, spectra are typically acquired by centering on the target in imaging mode, then moving the slit and grism into the optical

Table 3.1: Palomar AO spectroscopic observations

UT date	Time	Target	Type	Spectral range ^a	Airmass	Diam. ^b	Sub-Earth ^c
26 Sep 1999	07:17–07:24	Titan	imaging	K'	1.47–1.43	0.84	55.5, –20.6
26 Sep 1999	07:58–08:11	Titan	spectra	2.03–2.37	1.29–1.25	0.84	56.2, –20.6
26 Sep 1999	08:41–08:44	HD 1461	spectra	2.03–2.37	1.37–1.38	-	-
26 Sep 1999	09:16–09:35	Titan	spectra	2.03–2.37	1.10–1.08	0.84	57.4, –20.6
26 Sep 1999	10:03–10:13	Titan	spectra	2.03–2.37	1.06–1.06	0.84	58.1, –20.6
20 Jul 2000	11:40–11:48	HD 20065	spectra	2.10–2.32	1.51–1.46	-	-
20 Jul 2000	11:57–11:59	Titan	imaging	K'	1.62–1.61	0.74	295.2, –23.8
20 Jul 2000	12:05–12:09	Titan	spectra	2.10–2.32	1.56–1.55	0.74	295.4, –23.8
20 Jul 2000	12:28–12:32	HD 17163	imaging	K'	1.34–1.33	-	-
20 Jul 2000	12:32–12:34	HD 17163	imaging	K _s	1.32–1.32	-	-
20 Jul 2000	12:39–12:41	HD 22686	imaging	K _s	1.57–1.56	-	-
20 Jul 2000	12:41–12:44	HD 22686	imaging	K'	1.56–1.55	-	-
20 Jul 2000	12:51–12:53	Y5546	imaging	K'	1.79–1.80	-	-
20 Jul 2000	12:53–12:55	Y5546	imaging	K _s	1.80–1.81	-	-
20 Dec 2001	06:33–06:37	Titan	imaging	K _s	1.03–1.03	0.87	92.5, –25.5
20 Dec 2001	07:07–07:34	Titan	spectra	2.10–2.32	1.04–1.06	0.87	93.2, –25.5
20 Dec 2001	07:50–07:55	HD 32923	spectra	2.10–2.32	1.06–1.06	-	-
20 Dec 2001	09:22–09:51	Titan	spectra	2.10–2.32	1.32–1.46	0.87	95.3, –25.5
20 Dec 2001	09:59–10:05	HD 32923	spectra	2.10–2.32	1.36–1.38	-	-

a. Recorded spectral range (μm) or filter name.

b. Apparent diameter of Titan ($''$).

c. West longitude and latitude of the sub-Earth point ($^\circ$).

path. However, the position angle of the entrance slit and the orientation of the grism are not precisely reproducible after such moves. In most cases, we therefore acquired all spectra in a given set (Titan, sky, calibrator star, sky) without moving either the slit or grism. To accomplish this, Titan was initially centered $0''.6$ to the east of the measured slit location while in imaging mode. The slit (with a position angle of $0^\circ \pm 2^\circ$) and grism were then installed, and the first of a set of 120-s spectral integrations was begun. After each integration, the telescope was commanded $0''.10$ or $0''.12$ east, and the next integration begun, thus gradually sampling every location on Titan’s disk. Several effects lead to uncertainty in the actual offset between spectra, the most important being differential flexure between the science and wavefront-sensing light paths on the AO bench. This causes AO targets to drift linearly on the PHARO focal plane, at a rate of $\sim 0''.0002 \text{ s}^{-1}$. Depending on the direction of the drift, Titan’s disk was covered in 8–12 pointings.

After scanning the slit across Titan’s disk, the telescope was offset $60''$ north or south of Titan and several night-sky spectra with the same integration time were obtained. These were used to correct the detector bias, dark current, and atmospheric thermal and line emission recorded in the Titan spectra. With the slit and grism still in place, the telescope was slewed to a nearby solar analogue star (spectral class G0–G5, within 3° of Titan), and

several 60-s spectra of the star acquired with the AO feedback loops open. Finally, the telescope was offset $60''$ and several 60-s night-sky spectra were recorded, for calibration of the solar analogue spectra.

The entire observing sequence was repeated twice on both 26 September 1999 and 20 December 2001. A more limited set of observations was taken on 20 July 2000, consisting only of an imaging sequence, three 120-s spectra with the slit centered on Titan's central meridian, and calibration spectra. The grism and slit were also accidentally moved between Titan and calibrator star observations on that night, resulting in poor correction of the interference fringes which are superimposed on all spectra.

The observing conditions were photometric on 26 September 1999 and 20 July 2000 and marked by variable thin cirrus on 20 December 2001. Immediately following the Titan observations, three bright photometric standard stars (HD 17163, HD 22686, and Y 5546) were imaged on 20 July 2000. The AO feedback loop was left open to avoid saturation and 5 1.8-s images, in each of 4 positions on the detector, were acquired of each star through both K' and K_s filters. A summary of the observations is given in Table 3.1.

3.3 Data reduction

3.3.1 Images

Standard near-infrared image processing techniques were applied to the Titan images. Each set of dithered images was first grouped according to the location of Titan on the detector. For each location, a pixel-by-pixel median of the images not included was calculated and subtracted from each image in this subset, thus correcting for the detector bias, dark current, and the sky background. All images were then divided by a map of the relative pixel gains (the flat-field map), which was calculated from the average of bias and dark current subtracted twilight sky images taken through the appropriate filter on the same night. Finally, pixels with abnormal gain properties, as determined from twilight sky images taken over a wide range of sky brightness, were replaced by the median of the surrounding good pixels.

The geometric center of Titan's disk was next determined for each image in the set. The technique found to be most accurate at the high signal-to-noise ratio (SNR) of these broad-band images ($> 150 \text{ pix}^{-1}$ on the disk) was to fit a circle to Titan's limb. All

pixels within 1% of one-half the peak intensity of the disk were identified, and the sum of the squares of the distance between the center of these pixels and the nearest point of a circle was numerically minimized, solving for the circle’s position and radius. Monte-Carlo simulations of the technique demonstrate that at this SNR, the median random error in the determination of the disk of the disk center is 0.05 pix (1 milliarcsecond, mas). The actual uncertainty in Titan’s position on the detector is therefore dominated by systematic effects, particularly the presence of high contrast features on Titan’s disk. The feature capable of inducing the strongest centering bias would be a hemispheric albedo contrast, due either to surface albedo or the haze distribution. We estimate the systematic centering error by constructing a model of Titan’s disk with the strongest hemispheric contrast consistent with each recorded images, convolving this synthetic image with the estimated PSF (see Sec. 3.4.3) and calculating the apparent shift in the disk center. This leads to an upper limit in the systematic centering error of 0.9 pix (23 mas) for the 26 September 1999 images, which display a strong east-west albedo contrast, 0.7 pix (18 mas) on 20 July 2000, and 0.4 pix (10 mas) on 20 December 2001.

With Titan’s location determined, the images were shifted to a common center by adding a phase ramp to the Fourier transform, then transforming back to the image domain. This technique allows one to perform a sub-pixel shift while keeping the power spectrum of the image unchanged. The shifted images were then averaged to produce three nightly-mean images of Titan, displayed in Figure 3.1.

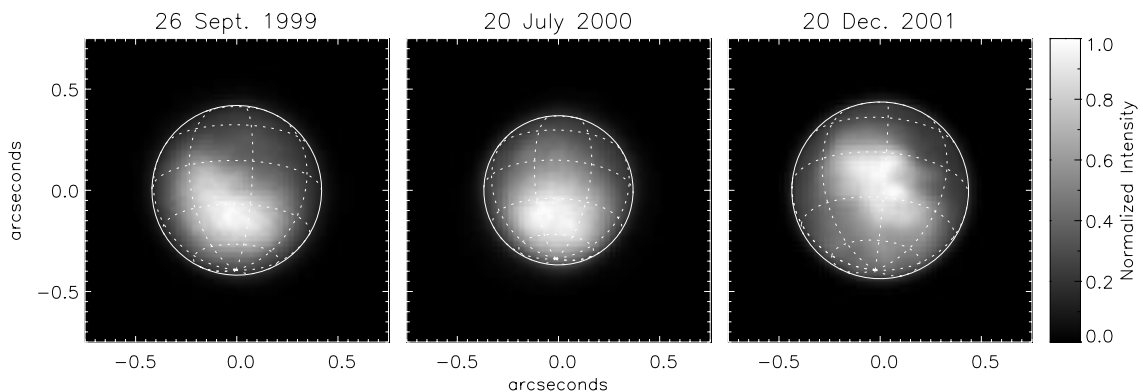


Figure 3.1: Broad-band K_s and K' images of Titan on the three nights of observation. Each image has been scaled independently to highlight subtle surface albedo patterns. Titan’s varying size and perspective are indicated by lines of latitude every 30° and longitude every 45° .

The initial processing steps applied to the photometric standard star images taken on 20 July 2000 were identical to those applied to the Titan images. However, rather than centering and averaging the images, the sum of the detector counts within a $10''$ radius of the centroid was determined for each frame, and the mean of these values used to establish the apparent instrumental flux of each star. The photometric zero-point and extinction per unit airmass in both K' and K_s were then determined by fitting the three standard star observations, allowing us to photometrically calibrate the 20 July 2000 Titan images to an accuracy of 5% . The same photometric factors were applied to the 26 September 1999 K' and 20 December 2001 K_s images for which no standard stars were observed, but the resulting calibration is only approximate.

3.3.2 Spectra

The process of transforming raw two-dimensional spectra of Titan and a solar analogue star to calibrated albedo spectra of known locations on Titan's disk required the following general steps. The precise alignment of the slit and grism relative to the detector, and the wavelength scale of each set of observations, were first determined from summed raw spectra. Each Titan and stellar spectrum was then corrected for detector, instrumental, and atmospheric effects, and the one-dimensional spectrum of Titan at each location along the slit extracted and divided by the stellar spectrum. Finally, the pointing location and photometric corrections of each Titan spectrum were determined by cross-correlating the image recorded through the slit with broad-band images taken the same night.

Spectra acquired with the PHARO camera are dispersed along the x -axis of the detector, with the projection of the entrance slit falling roughly parallel to the y -axis. Following movements of the slit and grism wheels, however, the alignment of these optical elements in PHARO can be uncertain by up to several degrees. Additionally, the projection of the slit on the PHARO detector is somewhat curved by optical distortions. Atmospheric OH emission lines recorded in long-exposure spectra provide a convenient fiducial with which to measure the slit angle and curvature. To maximize the SNR of the sky lines, we subtracted a mean of several 120-s dark frames from every Titan and night-sky spectrum in each set of observations, and averaged these dark-subtracted frames. The mean trace of the sky lines was then determined by cross-correlating each row of the resulting image with an arbitrary row near the center of the detector (ignoring the portion of the slit occupied by Titan),

then fitting a second order polynomial in relative offset x as a function of row y .

A similar procedure was used to measure the alignment of the grims with respect to the detector, and the optical distortion in the spectral dimension. A mean of the 60-s night-sky spectra taken immediately after the calibrator star observations was first subtracted from each stellar spectrum. All corrected calibrator star spectra in a set of observations were then averaged, and each column of the resulting image was cross-correlated with the central column. A second-order polynomial was then fit to the relative offsets in y as a function of column x .

A third step performed prior to the processing of individual Titan and calibrator star spectra was to determine the wavelength scale of each set of observations from the OH emission lines. The average of all dark-subtracted Titan and night-sky integrations was resampled using bilinear interpolation to cancel the measured slope and curvature in both axes. A high SNR sky spectrum was calculated by averaging all rows greater than $2''$ from Titan's location on the slit, and the locations of the 6 brightest emission lines determined by fitting one-dimensional Gaussian functions to them. A linear wavelength scale was finally fit to the locations and known wavelengths (Chamberlain and Smith, 1959) of these OH emission lines.

Following these preliminary steps, each Titan and calibrator star spectrum was processed individually. Spectra were first checked for cosmic rays, and the affected pixels replaced by the median of the surrounding good pixels. The 2–5 120-s night-sky integrations taken immediately after the Titan spectra were averaged, and this mean sky spectrum subtracted from Titan frame. Similarly, a mean of 60-s sky spectra was subtracted from each calibrator star integration. This step corrected for the detector bias and dark current, as well as subtracting the line and thermal sky emission which are superimposed on the target spectra. All spectra were next divided by the same K_s or K' flat-field map used for that night's images, correcting the detector's pixel-to-pixel gain variations. Bad pixels were replaced by the median of the surrounding values.

Both the Titan and stellar spectra were next resampled to align the spatial and spectral axes with the detector y and x axes. As was the case for the wavelengths scale determination, this resampling was done with the origin (the location at which the shift in both dimensions was zero) near the middle of Titan's spectrum, thus minimizing the loss of spatial and spectral resolution caused by the bilinear interpolation of adjacent pixel values. Some

residual sky emission remained visible in the Titan spectra at this stage, due to the changing atmospheric conditions during the observations. The residual sky emission was determined by averaging the spectrum $2''$ – $4''$ to either side of Titan along the slit, and subtracting this residual spectrum from each row. This step was not necessary for the higher SNR stellar spectra.

The processed calibrator star frames were averaged, and a one-dimensional stellar spectrum extracted by taking the mean over all illuminated rows, weighted by the relative flux in that row. By dividing every row of the Titan spectra by this spectrum of a solar analogue taken under identical conditions, the spectrally variable instrumental and atmospheric response were calibrated out, leaving Titan spectra in units proportional to albedo. In particular, strong interference fringes are present in the uncalibrated spectra, superimposed on both the Titan and stellar spectra due to monochromatic internal reflections in the detector. Division by the solar analogue spectrum successfully eliminates the fringes if the grism and slit were not moved between Titan and stellar observations. Some fringes remain in the 20 July 2000 Titan spectra due to the very slight (~ 1 pix) mis-match in wavelength between Titan and calibrator star spectra.

Each row of the processed Titan spectra records the spectrum at one location along the entrance slit. Since the detector platescale oversamples the diffraction-limited spatial resolution of the Hale telescope, spectra were next averaged along-slit by a factor of 2–3, leading to a final spatial sampling of $0''.080$ on 26 September 1999 and $0''.076$ on 20 July 2000 and 20 December 2001. The uncertainty in the spectra due to electronic and photon noise was estimated from the the full range of the pixel values included in the spatial average at each wavelength.

The final step of the reduction sequence was to determine the pointing location of each spectrum with respect to the center of Titan’s disk, by comparing the spectrum recorded through the slit with the K' or K_s images taken the same night. As noted previously, the telescope was commanded $0''.10$ or $0''.12$ east between each Titan integration, but flexure of components on the AO bench and inaccurate control of the articulated mirrors which direct light to the wavefront sensor caused this offset to be uncertain. Experiments performed with an internal calibration source demonstrate that the gradual drift of the AO corrected image on the PHARO focal plane due to flexure is linear on timescales of an hour or less. The effect of inaccurate steering mirror control is less well constrained, but probably contributes

random offsets between spectra of less than $0''.02$. The sum of the commanded offset and the gradual $\sim 0''.0002 \text{ s}^{-1}$ drift due to flexure therefore causes Titan to follow a nearly linear trajectory across the entrance slit.

Each Titan spectrum was multiplied by the imaging filter transmission function, and summed over wavelength to produce one-dimensional images of Titan as seen through the $0''.13$ -wide entrance slit. The iterative routine AMOEBA (Press *et al.*, 1992) was then used to minimize the square of the difference between the set of slit images and the nightly broad-band image, assuming a linear offset between successive spectra. Five parameters were solved for: the location of the slit center with respect to that of Titan for an arbitrary spectrum (2 parameters), the offset in arcseconds between successive spectra (2 parameters), and a photometric scaling factor. This scaling factor, corrected for the flux admitted by the imaging filter but not sampled by the spectra which we calculated from the disk integrated spectra of Fink and Larson (1979), allowed us to photometrically calibrate the Titan spectra to match the calibrated images. The sets of central meridian spectra taken on 26 September 1999 and 20 July 2000 were navigated in a similar fashion, solving for only 3 parameters: the north-south position, drift rate, and photometric scaling factor. Finally, several of the individual spectra taken on 20 December 2001 were clearly affected by passing terrestrial clouds. The procedure was modified for these data, allowing the minimization algorithm to correct the photometry of each slit image independently. Those spectra whose apparent flux was reduced by more than a factor of two (located along Titan's western limb) were excluded from the analysis.

3.4 Analysis

3.4.1 Spectral diversity

Titan's near infrared albedo results largely from the absorption of solar radiation by CH_4 and H_2 , and scattering of radiation from particles (both photochemically produced haze and possibly from condensate clouds) and from the surface. We use the strongly wavelength-dependent absorption features of methane in Titan's atmosphere as a vertical filter with which we can resolve the altitude of hazes and clouds. Deep in the saturated absorption band at $2.17\text{--}2.25 \mu\text{m}$, only sunlight scattered off haze in Titan's stratosphere is detected. Shorter wavelengths sample progressively deeper levels of the atmosphere, allowing scattering in the

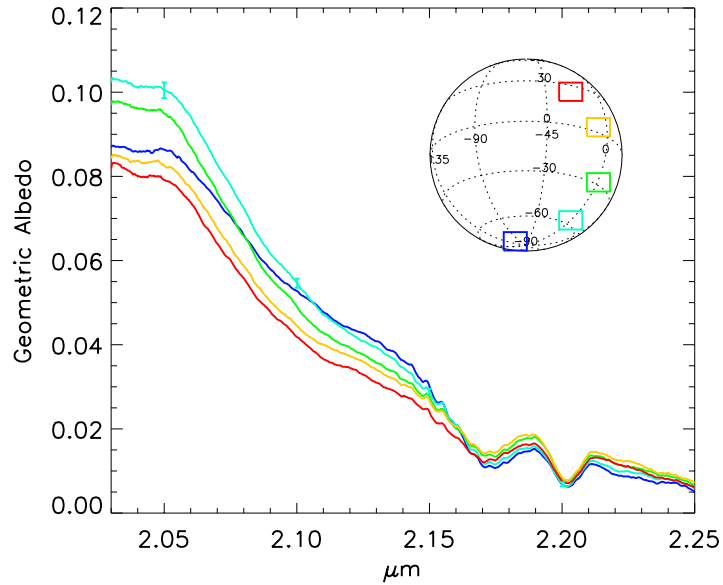


Figure 3.2: Five spectra of Titan’s disk on 26 September 1999, chosen to sample similar incidence angles through Titan’s atmosphere at a variety of latitudes. They have been smoothed for clarity. Equatorial spectra are brightest deep in the 2.25 μm absorption band, indicating a thicker stratospheric haze layer above the bulk of Titan’s atmospheric methane. Spectra at high southern latitudes, in contrast, rise steeply on the edge of the methane band (from 2.17 to 2.12 μm), revealing a region of enhanced scattering deep in Titan’s atmosphere, yet distinct from variations in surface albedo which dominate the spectra shortward of 2.12 μm .

troposphere to affect the flux shortward of 2.17 μm , and albedo variations on Titan’s surface to dominate shortward of 2.12 μm . A comparison of spectra of various regions on Titan’s disk on 26 September 1999 (Fig. 3.2) illustrates the diversity of spectra recorded across the disk. Equatorial spectra are brightest at 2.17–2.25 μm , while spectra of regions near Titan’s south pole appear brighter at 2.12–2.16 μm . Near 2.10 μm , spectra cross one another again as local surface albedo begins to dominate.

Low-resolution images of Titan’s surface, troposphere, and stratosphere can be created by integrating each spectrum over a narrow wavelength range and displaying the resulting albedo over projections of the spectral apertures (Fig 3.3). Titan’s surface is most clearly seen at 2.02–2.05 μm , but this spectral region was only sampled in 1999. The 2.10–2.12 μm range was observed on every run, and remains weakly sensitive to Titan’s surface while also displaying a concentration of scattering particles near Titan’s south pole. Summed

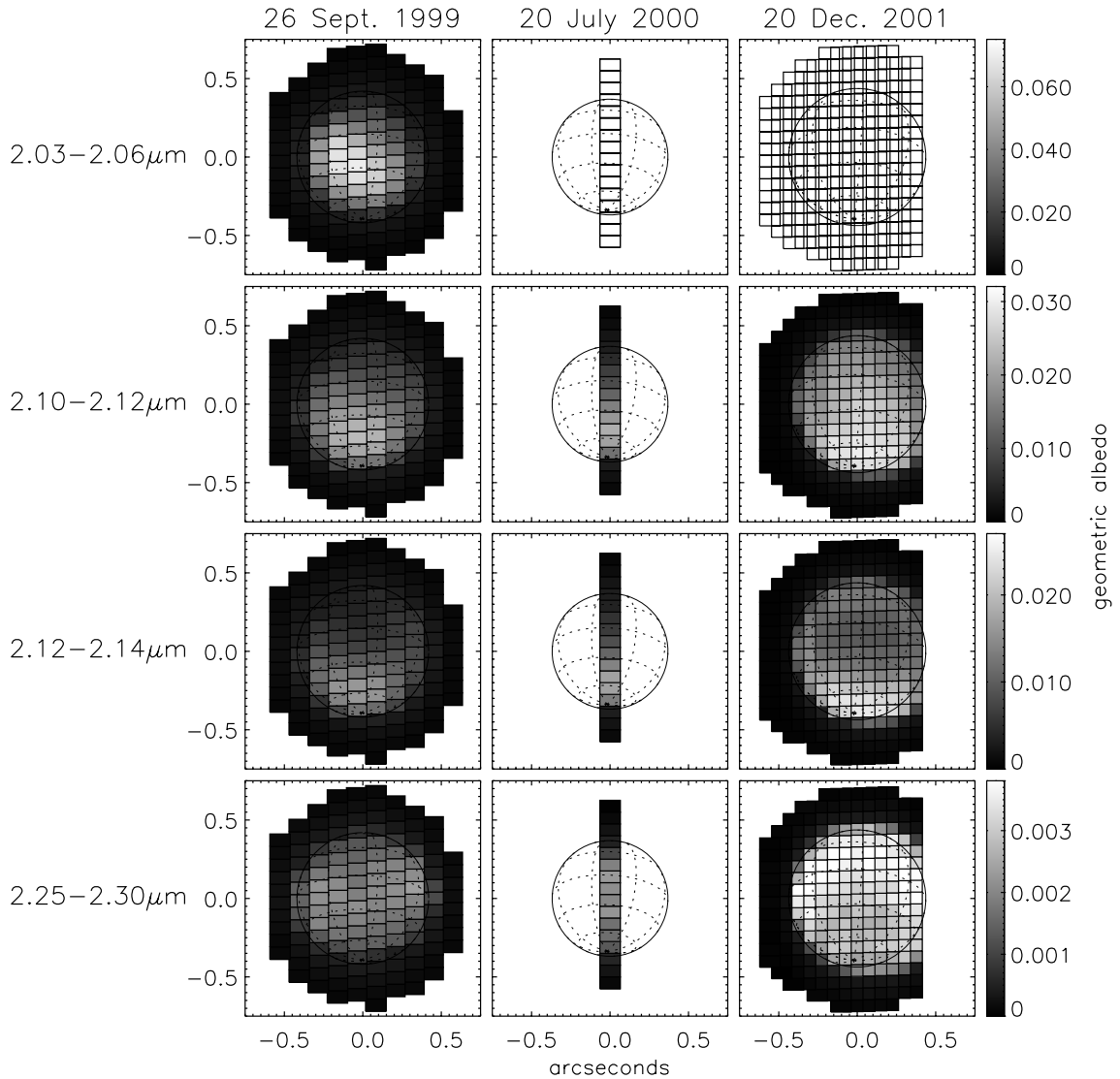


Figure 3.3: Narrow-band images of Titan created by averaging the spectrum recorded in each aperture over four narrow wavelength ranges. High contrast features on Titan’s surface can be clearly seen at $2.02\text{--}2.05\ \mu\text{m}$ on 26 September 1999. The surface contributes only weakly to the $2.10\text{--}2.12\ \mu\text{m}$ images. A region of bright scattering particles near Titan’s south pole is most clearly seen at $2.12\text{--}2.14\ \mu\text{m}$, where the atmosphere is opaque to Titan’s surface. Obvious changes can be seen in the highest haze layers, seen most clearly in the $2.25\text{--}2.30\ \mu\text{m}$ images. The apparent brightening of Titan at all wavelengths is due to the improved AO correction of the 2001 observations.

over 2.12–2.14 μm , all traces of Titan’s surface disappear and the bright atmospheric feature near Titan’s south pole is more clearly seen. Only a region of bright scattering near the tropopause, present above Titan’s south pole but thin or absent over the equator and mid-latitudes, can account for this feature. The most dramatic change in the appearance of Titan’s atmosphere between 1999 and 2001 can be seen in the 2.25–2.30 μm images, which record only the highest haze layers (> 110 km altitude.)

3.4.2 Radiative transfer

The strategy we adopt to derive Titan’s surface albedo and the opacity structure of the overlying atmosphere is to forward model the spectra, starting with a parametrized description of Titan’s surface and atmosphere. Using the radiative transfer model of Griffith (1991), we compute the predicted reflectance spectrum at every location on dense grid covering Titan’s disk, which we then spatially convolve by an estimate of the PSF and sample at the locations of the spectral apertures.

The equation of radiative transfer is approximated using the doubling and adding technique (Hansen and Travis, 1974). Titan’s atmosphere is modeled as 147 layers ranging in thickness from 0.5 km near Titan’s surface to 50 km at 1200 km altitude, using the temperature-pressure model of Lellouch (1990). Absorption due to CH_4 and H_2 is calculated line by line, and converted to correlated K-coefficients for the actual calculations. The CH_4 mixing ratio in the lower troposphere is assumed to be 0.07 (60% relative humidity at the surface), up to the height at which this equals the saturation value. The saturation mixing ratio is then followed to the tropopause at 40 km, above which the saturated tropopause value of 0.017 is followed (Lellouch *et al.*, 1989). Rayleigh scattering by the gas is included, as is Mie scattering by haze (0.6 μm particles with tholin optical constants). CH_4 cloud particles are assumed to scatter isotropically, with a single-scattering albedo of 0.98.

3.4.3 PSF estimation

An estimate of the mean long-exposure PSF was determined for each set of observations by modeling the broad-band images acquired immediately prior to the spectrum observations. The nightly mean K' or K_s image (Fig 3.1) was modeled by convolving a blank disk at the known location of Titan by a PSF consisting of a sum of 3 Gaussian functions. A sum of

Gaussians is clearly only a rough approximation to the true PSF, but its purpose here was primarily to estimate the power and width of the halo component, which is expected to be both smooth and symmetric. The structure of the PSF core and possible diffraction rings were of much less concern. The full-width at half maximum (FWHM) of the narrowest Gaussian was fixed at $0''.087$, that expected for a diffraction-limited PSF at $2.1 \mu\text{m}$ wavelength. The widths of the other two, and their relative contribution to the normalized PSF, were allowed to vary, and were optimized using the AMOEBA algorithm (Press *et al.*, 1992) to minimize the square of the difference between the predicted and observed halos (the region beyond the solid limb of Titan). The optimized PSFs were found to closely reproduce the observed halos, thus providing a robust estimate of the contribution of distant regions of Titan to individual spectral apertures.

3.4.4 Model optimization

Both Voyager and Earth-based observations have found Titan’s haze to be zonally symmetric. This is to be expected from the long response time of the stratosphere to seasonal forcing, and the slow rotation of the satellite. Spatially resolving Titan’s disk therefore allows us to sample a given haze column at a variety of emission angles. This reinforces the ability to constrain the vertical haze opacity profile, and to distinguish low haze from bright surface regions. The recent identification of discrete condensate clouds near Titan’s south pole (Brown *et al.*, 2002; Roe *et al.*, 2002) indicates that tropospheric clouds cannot be treated in the same way.

The spectral modeling was performed in several steps, gradually increasing the number of free parameters; we describe here the most complex, final model. Titan’s atmosphere is divided into 5 zonal bands whose widths roughly match the spatial resolution achieved under the worst conditions. The haze in each band is parametrized in terms of the optical thickness in 4 layers between 40 km and 1265 km altitude, plus a fifth layer in the troposphere whose altitude is allowed to vary. Each latitude band is further divided into longitudinal zones of width $\sim 45^\circ$, between which only the surface albedo is allowed to vary. 14 independent surface albedo patches cover Titan’s visible disk (Fig. 3.8). A maximum of 6 free parameters are therefore used to describe Titan’s surface and atmosphere at each location on the disk, for a maximum total of 39 free parameters.

The observed spectra constitute a set of N measurements of the geometric albedo $y_i =$

y_1, \dots, y_N at location \mathbf{r} and wavelength λ , with an associated uncertainty σ_i . We fit these spectra using the above model with M adjustable parameters $a_k = a_1, \dots, a_M$. For a given vector of parameters $\mathbf{a} = (a_1, \dots, a_M)$, we transform this model into a prediction of the spectrum in each aperture $y(\mathbf{r}, \lambda; \mathbf{a})$ as follows. We first use the radiative transfer model to calculate the predicted spectrum every 0.010 on a $1'' \times 1''$ grid centered on Titan. The emission angle for which the spectra are calculated varies between grid points, even within latitude bands and surface-albedo patches. The resulting three-dimensional dataset (a spectrum at every grid point) is then spatially convolved by the estimated PSF, and sampled at the locations of the actual spectral apertures. Assuming normally distributed errors σ_i , the maximum likelihood estimate of the model parameters \mathbf{a} will be achieved by minimizing the χ^2 merit function

$$\chi^2(\mathbf{a}) = \frac{1}{N - M} \sum_{i=1}^N \left(\frac{y_i - y(\mathbf{r}_i, \lambda; \mathbf{a})}{\sigma_i} \right)^2. \quad (3.1)$$

We used the Levenberg-Marquardt algorithm (Press *et al.*, 1992) to optimize the M adjustable model parameters described above to minimize this merit function.

3.5 Results

3.5.1 Mean atmosphere

Though it is clear that Titan’s haze, clouds, and surface albedo vary across the visible disk, disk average haze properties provides a useful point of reference, permitting comparison

Table 3.2: Radiative transfer model parameters

Model	Date	N^a	M^b	Wavelength (μm)	χ^2
Mean atmosphere	26 Sep 1999	89×105	5	2.12–2.30	18.4
	20 Jul 2000	26×105	5	2.12–2.30	11.5
	20 Dec 2001	150×105	5	2.12–2.30	9.0
Zonal atmosphere	26 Sep 1999	89×105	25	2.12–2.30	13.8
	20 Jul 2000	26×105	25	2.12–2.30	6.0
	20 Dec 2001	150×105	25	2.12–2.30	6.0
Atm. & surface	26 Sep 1999	89×120	39	2.03–2.05, 2.12–2.30	13.3

a. Number of spectral apertures, times the number of wavelengths fit.

b. Number of free parameters in the model.

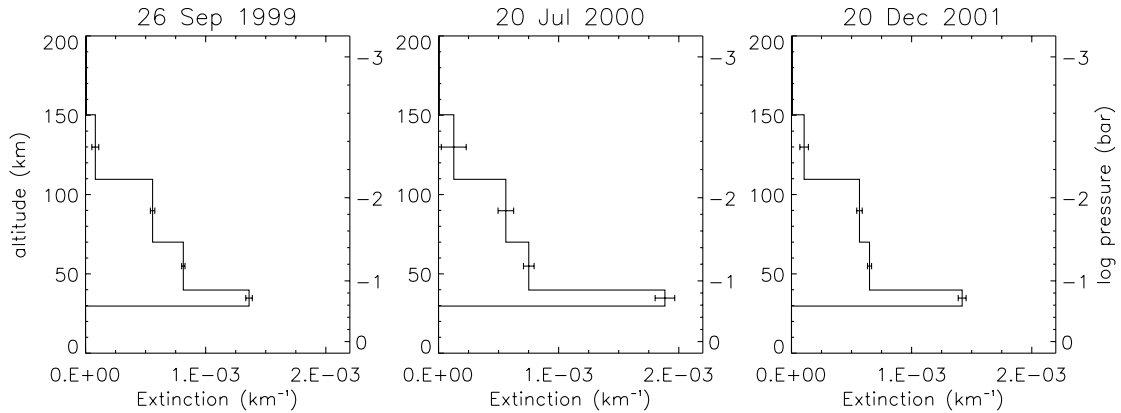


Figure 3.4: Average haze extinction profiles on each night. No haze or cloud layer is necessary below 30 km. Error bars represent $1\text{-}\sigma$ random error. To within the errors, the mean opacity distribution of the main haze layer (> 40 km) appears to have remained unchanged over the two years spanned by these observations.

with previous disk integrated spectroscopy. We therefore first fit the observed spectra using a single set of parameters to describe the vertical haze profile at all latitudes, while performing all other aspects of the model optimization as described in section 3.4. Note that this average model is therefore weighted not by flux, as an unresolved spectrum would be, but by area (since the individual spectra are evenly distributed in area.) Only the spectral region insensitive to Titan’s surface ($2.12\text{--}2.30\ \mu\text{m}$) is used in the fit.

The resulting fit between the predicted spectra and those observed is not particularly good (see Table 3.2.) However, several interesting features of Titan’s haze are apparent (Fig. 3.4). In a global mean sense, the total optical depth of scatterers in Titan’s lower stratosphere remained constant over the two years of observations. The total haze optical depth was $\tau = 0.072 \pm 0.005$ on 26 September 1999, $\tau = 0.076 \pm 0.016$ on 20 July 2000, and $\tau = 0.070 \pm 0.006$ on 20 December 2000. The $1\text{-}\sigma$ uncertainties listed here and displayed in the figures are the random error due primarily to electronic and photon noise in the raw spectra. Not included is an additional systematic uncertainties, the most important being the uncertain flux calibration of the spectra which we estimate to be in error by less than 15% on 26 September 1999 and 20 December 2001, and 5% on 20 July 2000.

The haze extinction appears to increase with decreasing altitude to 30 km above Titan’s surface, below which no haze is necessary to adequately model the spectrum. However, haze or clouds between 30 and 40 km altitude are required to correctly fit the spectra (Fig. 3.7).

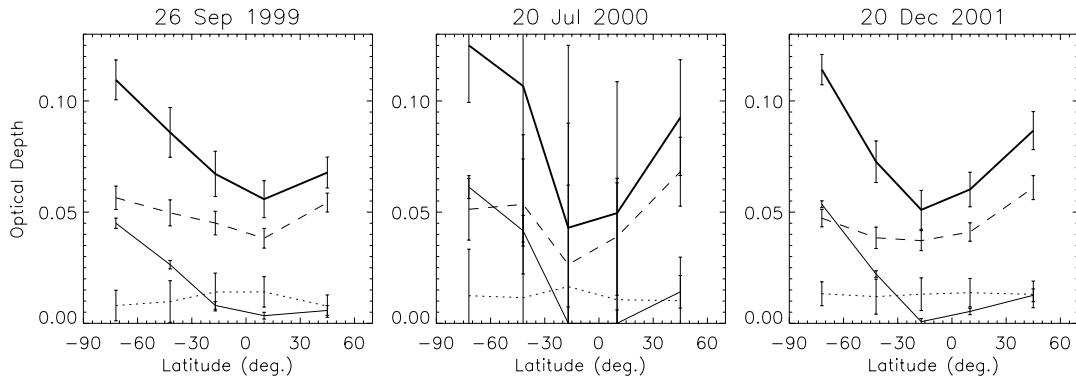


Figure 3.5: Summary of the optical depth of haze measured as a function of altitude and latitude. *Dotted line*: > 110 km. *Dashed line*: 40–110 km. *Thin solid line*: 30–40 km. *Thick solid line*: Total scattering optical depth. Error bars represent $1\text{-}\sigma$ random error. Though the south polar tropopause scattering layer has remained unchanged over two years, a gradual shift to the north can be seen in the main haze layer above 40 km.

3.5.2 Zonal haze model

Gradually increasing the complexity of the model, we next divide Titan’s atmosphere into five zonal bands. We continue to ignore the surface by fitting only the $2.12\text{--}2.30\ \mu\text{m}$ region of the spectra. Figure 3.5 summarizes the evolution of the vertical distribution of the haze over the two years of observations, while vertical profiles near Titan’s south pole and equator on 26 September 1999 and 20 December 2001 are shown in Fig. 3.6.

The most striking feature of the latitude-resolved haze profiles is the strongly scattering layer at 30–40 km altitude, present only at high southern latitudes. Though the layer is optically thin ($\tau \approx 0.05$), it accounts for half of the total scattering optical thickness at Titan’s south pole. Above this tropospheric scattering layer, the main haze deck exhibits a distinctly different latitude dependence. At 40–110 km, aerosols appear evenly distributed in latitude in 1999, while a clear shift towards Titan’s northern limb has occurred by December 2001. The highest haze layers to which these observations are sensitive, above 110 km, appear thicker above Titan’s equator in 1999, but more evenly distributed by 2001. Haze profiles fit to the central meridian spectra taken 20 July 2000 are included in Fig. 3.5 to demonstrate that they are consistent with a gradual transition between the 1999 and 2001 aerosol distributions. However, the absence of a variety of emission angles sampling each zonal band of the model leads to far larger uncertainties in the retrieved haze optical depths.

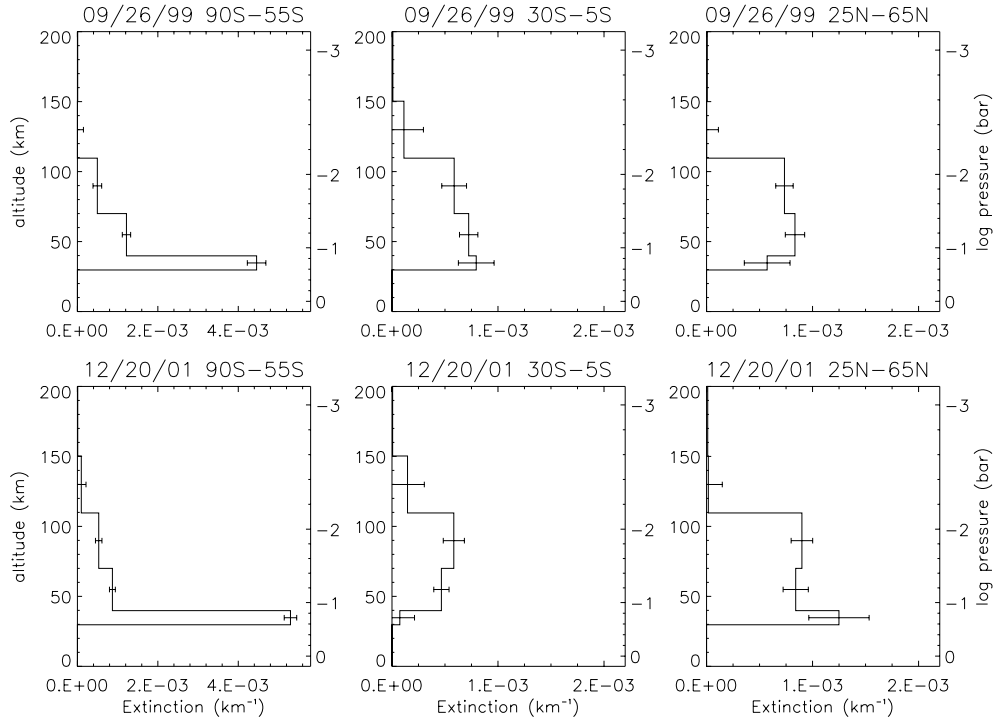


Figure 3.6: Sample haze profiles at 3 latitudes on Titan, on 26 September 1999 and 20 December 2001. The conspicuous scattering layer at 30–40 km altitude is reduced in thickness by at least a factor of 4 north of 30°S. Error bars represent 1- σ random error. Note the change in extinction scale between the plots.

In both the mean atmosphere and zonal models, the altitude of any tropospheric scattering layer is left as a free parameter, which is optimized along with its optical depth and the vertical distribution of the overlying stratospheric haze. Though the spectral fits indicate that the optimum altitude of a tropospheric scattering layer is 30–40 km, this result is not independent of the derived stratospheric haze profiles.

To better constrain the altitude of the southern tropospheric scattering layer, we isolate its spectrum by subtracting spectra of Titan’s southern and northern limbs (Fig. 3.7). The residual shows a rapid rise in albedo between 2.17 and 2.14 μm . The residual is most closely fit by a layer of scattering particles at 30–40 km above Titan’s surface, with an optical depth of $\tau = 0.04 \pm 0.01$. This is slightly lower than was found in the zonal model optimization, since some opacity ($\tau \approx 0.01$) is present at this altitude in the northern limb spectra as well. The difference spectrum can equally well be fit by a region of scattered optically thick clouds with tops near 40 km, covering $2.7 \pm 0.7\%$ of the region sampled by the southern spectra. By fitting the difference between southern and northern limb spectra, the altitude

at which we locate the layer is independent of our interpretation of the overlying haze. The disadvantage of this method is that the optical depth of the layer is underestimated. The primary uncertainty in the altitude is due to the poorly constrained distribution of CH_4 in Titan’s stratosphere, which we assume to have a constant mixing ratio of 0.02 (Lellouch *et al.*, 1989). Below the tropopause scattering layer, Titan’s atmosphere appears free any widespread haze or cloud layers with optical thickness $\tau > 0.01$ at $2.0 \mu\text{m}$ (averaged over the $\sim 1200 \text{ km}$ projected spatial resolution), determined by inserting such a layer in the atmospheric model and testing for consistency with the observed spectra.

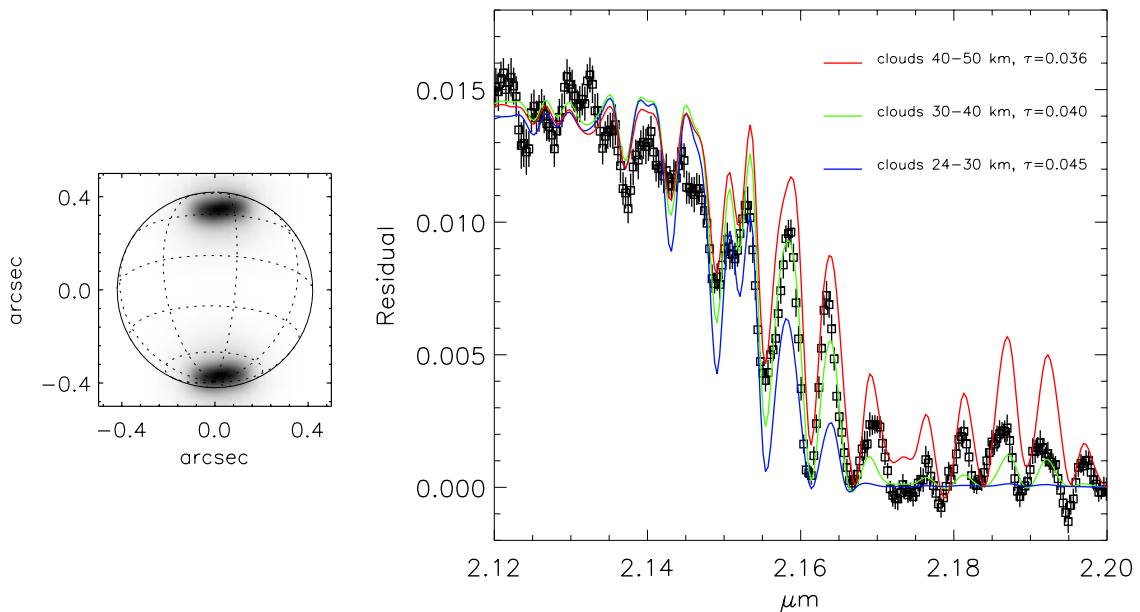


Figure 3.7: The difference between the mean of two southern and two northern limb spectra, fit with radiative transfer models. Their spatial weighting functions are displayed on the left. Model spectra were calculated with the identical geometry, and their difference fit to the residual. The extra flux in Titan’s south polar atmosphere can best be fit by the addition of an optical depth $\tau = 0.04 \pm 0.01$ scattering layer at 30–40 km altitude in the south. Equivalently, the layer could consist of scattered optically thick clouds with tops at 30–40 km altitude, covering $2.7 \pm 0.7 \%$ of the south polar region.

3.5.3 Surface albedo

The opacity of Titan’s atmosphere due to CH_4 and H_2 is sufficiently low at $\lambda < 2.12 \mu\text{m}$ for images and spectra of Titan to record light scattered at the surface. Uncertainty in

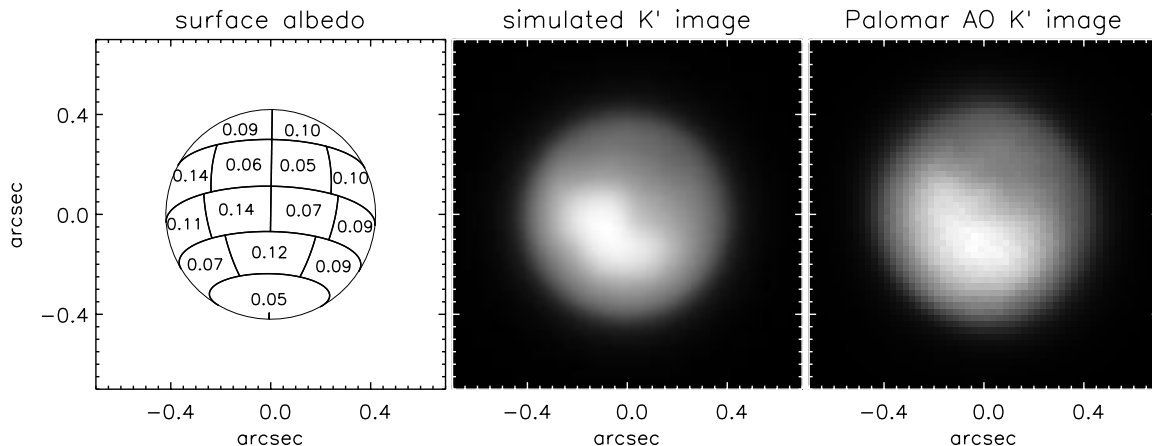


Figure 3.8: *left*: Titan’s surface albedo at $2.04 \mu\text{m}$, determined by optimizing a radiative transfer model to 89 spectra taken on 26 September 1999. The locations of the 14 independent surface regions is arbitrary. The atmosphere is divided into 5 zonal bands, in which the vertical haze distribution in 5 layers was simultaneously fit. The estimated uncertainty is 15%, dominated by the poor photometric calibration of the spectra. *center*: Model spectra at each location on Titan’s disk were multiplied by the K' transmission spectrum and spatially convolved by the estimated PSF, to produce this simulated K' image. *right*: Actual Palomar AO K' image of Titan taken at 07:24 UT on 26 September 1999.

the collision-induced absorption coefficients of $\text{H}_2\text{-N}_2$ leads to poor fits between the model spectra and those of Titan between $2.05\text{--}2.12 \mu\text{m}$ (Griffith *et al.*, 1998). Only our 26 September 1999 spectral observations recorded the region $\lambda < 2.05 \mu\text{m}$ over which we can reliably determine Titan’s surface albedo.

The surface albedo distribution determined by optimizing the full surface and atmospheric model described in Section 3.4.4 is presented in Fig. 3.8. Atmospheric parameters remain essentially unchanged from the atmosphere-only model fit, and no scattering layer between 5 and 30 km altitude is necessary to fit the spectra. The spectra provide no distinction between a bright surface and bright clouds below 5 km altitude.

Despite the coarse resolution and arbitrary locations of the patches into which Titan’s surface has been divided, the derived albedo distribution does an excellent job of reproducing the spectra observed on 26 September 1999. Several sample fits are presented in Fig. 3.9. A further encouraging result is the quantitative similarity between a simulated K' image of Titan computed from the surface albedo and haze distributions, and an actual image taken the same night (Fig. 3.8).

Titan’s surface displays strong albedo contrasts of at least a factor of two at regional

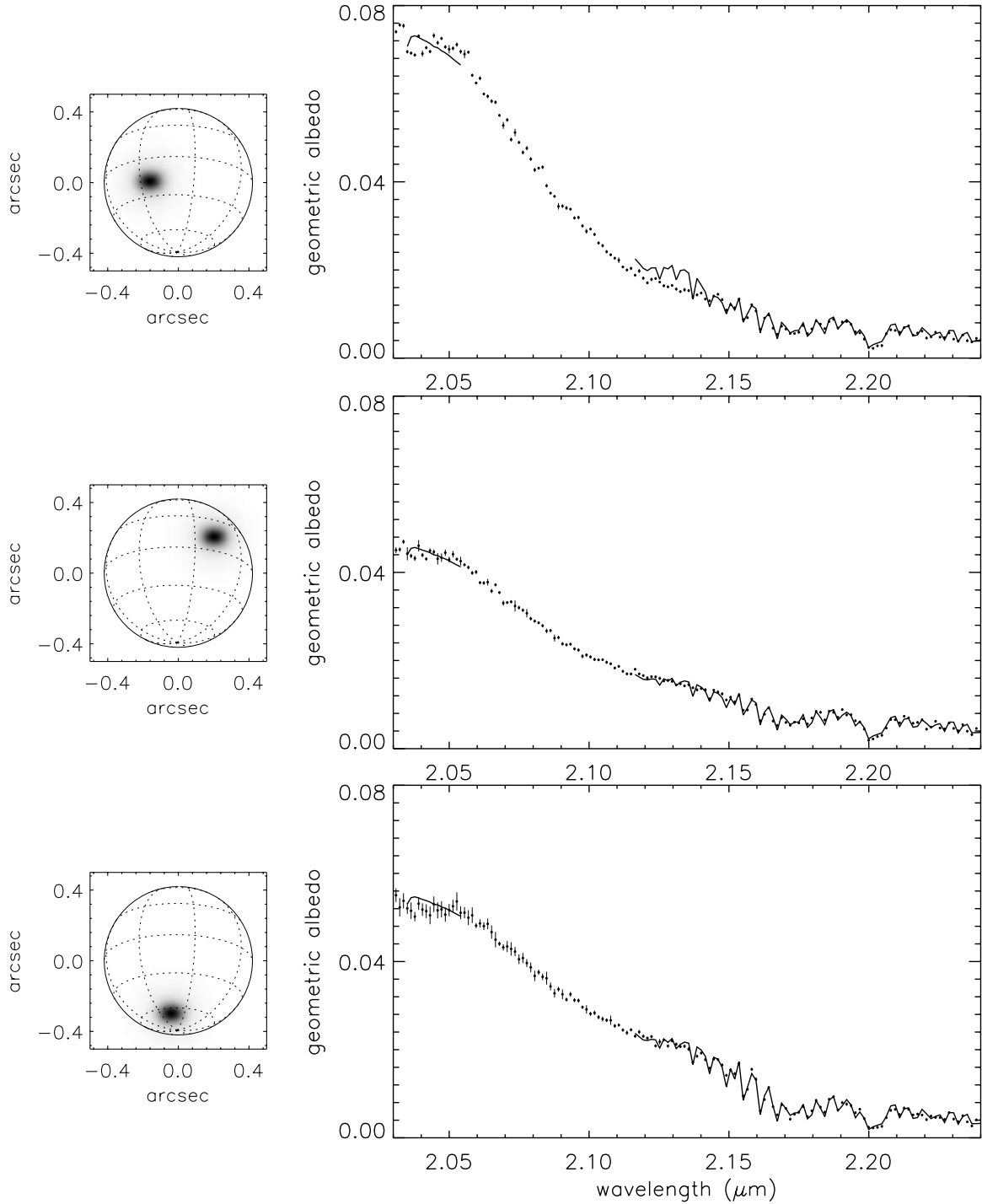


Figure 3.9: Sample model fits to three spectra taken 26 September 1999. The observed spectra are displayed as points, with 1- σ error bars which do not include the 15% photometric calibration uncertainty. The spatial weighting function of each spectrum is shown on the left. Optimized model spectra are indicated by solid lines. These three spectra were chosen to illustrate bright and dark surfaces (*top* and *center*) and the hazy south polar region (*bottom*).

spatial scales, despite the inevitable reduction in contrast imposed by an extended PSF. Though we attempt to correct for the PSF in our analysis by comparing a convolved synthetic image to the observations, the coarse resolution with which we parametrize the surface similarly reduces the recovered contrast. It is therefore quite startling that we find a range of albedos of nearly a factor of 3, from 0.05 ± 0.01 to 0.14 ± 0.02 .

3.6 Discussion

3.6.1 Seasonal change in Titan's haze

The gradual northward movement of haze in the main layer above 40 km altitude appears to be an expression of the advection of haze in Titan's stratosphere by meridional winds. General circulation models indicate that pole-to-pole thermally direct winds probably dominate Titan's stratospheric meridional circulation during most of the year (Hourdin *et al.*, 1995; Rannou *et al.*, 2002). Titan's seasonally varying north-south brightness asymmetry at visible wavelengths is one consequence of haze advection by meridional winds.

Since 1994, Titan's northern hemisphere has been darkening in the blue, evolving back towards the state observed by Voyager in 1980 and indicative of a thickening high haze layer (Lorenz *et al.*, 1999). By 1997, the optical thickness of high haze (> 160 km altitude, appearing dark in blue filters and bright in CH_4 bands) in the north exceeded that in the south, while the layers below appeared to lag behind (Lorenz *et al.*, 2001). More recent visible adaptive optics observations of Titan confirm this picture, finding the main haze layer (< 90 km) globally uniform as late as November 2001 (Ch. 2).

The spectral observations presented here are more sensitive to changes in the total optical thickness of the main haze layer than visible-light images, and they record subtle changes between September 1999 and December 2001. While the optical depth of haze above Titan's tropopause appears to have remained constant in the south polar and equatorial regions, it has increased by $20 \pm 5\%$ at 45°N . Rannou *et al.* (2002) suggest an elegant mechanism for the thickening of the main haze layer in the mid-latitudes of the winter hemisphere. The pole-to-pole meridional winds act as a conveyor belt for aerosols created high in the equatorial stratosphere, carrying them first north (during southern summer) along the detached haze layer, then down towards the winter pole. The thickening haze would then circulate southward at lower altitude, causing the observed increase in main

layer's optical depth in the northern mid-latitudes.

3.6.2 Tropopause cirrus

The brightly scattering region near Titan's south pole has been noted previously in both visible (Lorenz *et al.*, 1999; Young *et al.*, 2002; Ch. 2) and near-infrared (Coustenis *et al.*, 2001; Roe *et al.*, 2002) images of Titan, but its altitude was misinterpreted or constrained only to lie within the troposphere. We have demonstrated that the spectral signature of this scattering layer reveals it to be at the very top of the troposphere, at 35 ± 10 km. Significantly, this is well above the transient tropospheric clouds which populate the same region. The tops of the transient clouds, interpreted to be convective towers initiated by surface heating, were found to lie at 16 ± 5 km (Brown *et al.*, 2002), near the level expected for moist convection (Griffith *et al.*, 2000).

A surprising feature of the tropopause scattering layer is its apparent stability, despite the seasonal changes taking place in the main haze layer above. It changed in neither thickness nor extent between 1999 and 2001, remaining restricted south of $\sim 30^\circ\text{S}$. This same behavior was noted in the analysis of visible AO images of Titan in Ch. 2. The stability suggests that the aerosols which comprise the layer are either long-lived, or continuously replenished by a process which is not undergoing significant seasonal evolution.

Early suggestions that the layer might represent CH_4 or C_2H_6 condensation onto C_4N_2 ice-covered haze particles (Samuelson *et al.*, 1997) now seem unlikely, since the C_4N_2 source is expected to diminish rapidly as stratospheric temperatures rise in late spring. It also seems unlikely that the settling of haze from the main layer could lead to such a stable feature, during a season in which significant upward vertical motion is predicted (Hourdin *et al.*, 1995; Tokano *et al.*, 1999). The presence of tall convective clouds beneath the scattering layer, and a steady pole-to-pole circulation pattern, suggest another possibility. The tropopause scattering layer may be a region of cirrus-like CH_4 condensation clouds, related either to the upwelling of moist air in the convective plumes, or the regional upwelling of the summer pole. The later case would be analogous to optically thin tropical cirrus on the Earth, which form at the tropopause in the rising cell of the Hadley circulation (Kärcher, 2002). Higher spatial resolution observations will be required to distinguish between these various possibilities.

3.6.3 Surface

Resolved images of Titan through low-opacity spectral windows from 0.6 to 2 μm reveal high contrast, apparently permanent albedo features on its surface. However, the difficulty of analyzing broad-band (frequently deconvolved) images taken through an absorbing and scattering atmosphere has led to a lack of consensus on both the absolute albedos of features, and the contrast exhibited between bright and dark regions.

Early HST images of Titan's surface (Smith *et al.*, 1996; Meier *et al.*, 2000) were corrected for light scattered in Titan's stratosphere by subtracting a zonally averaged image, leaving no hope of recovering the absolute surface albedo. Most ground-based observers have instead relied on subtracting an image of Titan taken at a nearby wavelength sensitive only to the haze, but have stopped short of correctly modeling the absorption experienced by the residual light scattered from the surface (Combes *et al.*, 1997; Coustenis *et al.*, 2001; Ch. 2). Gibbard *et al.* (1999) estimate the absolute albedo of Titan's surface using a simple 3-layer radiative transfer model to interpret speckle interferometric images on two nights. Though an improvement over the previously described techniques, one weakness of theirs is in the optimization of the haze model, for which they effectively assume Titan's surface to have zero albedo near the edges of the disk. Consequently, the haze optical depth is overestimated to some degree, leading to an underestimate of the surface albedo and a possible overestimate of the surface contrast. Nevertheless, they find that the albedo of Titan's surface at 2.0 μm ranges from 0.05 to 0.13 at a spatial resolution of ~ 240 km.

The spectral modeling technique which we have developed in this chapter allows both the surface albedo and three-dimensional haze distribution overlying the surface to be determined simultaneously, at the expense of a loss of spatial resolution (due primarily to the reduced spatial resolution generally achieved with the longer exposures required for spectroscopy.) We find that the 2.0 μm surface albedo of the hemisphere centered on coordinates 57°W, 21°S ranges from 0.05 ± 0.01 to 0.14 ± 0.02 when averaged over spatial scales of ~ 1200 km. The mean surface albedo of this hemisphere of Titan (weighted by projected area) is 0.09 ± 0.01 .

The hemisphere of Titan viewed on 26 September 1999 includes the eastern extension of the bright, continent-like feature centered at approximately 100°W and the very dark region to its north-east. Though there is little actual overlap with the surface albedo maps

of Gibbard *et al.* (1999), we derive a consistent albedo for the bright region (of which they viewed the western half), and similar values for the darkest areas surrounding it. We therefore concur with their surprising result that the $2.0\ \mu\text{m}$ albedo of the large bright region is similar to that of the icy Galilean satellites, whose geometric albedos range from 0.10 (Europa) to 0.18 (Ganymede). The albedo of pure H_2O ice at $2.0\ \mu\text{m}$ varies widely as a function of grain size, but spans the range 0.10–0.25 at the conditions found on the icy Galilean satellites (Clark and Mc Cord, 1980). If the bright region on Titan represents exposed water ice with a similar grain structure, then its relatively high albedo argues that extensive regions must be kept free of the accumulation of dark atmospheric sediments, by either topography or active meteorological processes. In contrast, dark areas surrounding the bright surface feature have a $2.0\ \mu\text{m}$ albedo which is consistent with a surface covered by either hydrocarbons or expected atmospheric precipitates (Khare *et al.*, 1984, 1990).

3.7 Conclusions

The observations presented in this chapter comprise the first spatially resolved spectra of Titan at near-infrared wavelengths. They combine spatial and spectral resolution sufficient to simultaneously determine the vertical distribution of aerosols in Titan’s atmosphere and the albedo of the underlying surface.

Over the period of September 1999 to December 2001 (late southern spring on Titan), the changing distribution of aerosols in Titan’s stratosphere appears consistent with recent models in which haze is advected by thermally-direct meridional winds (Rannou *et al.*, 2002). However, a distinct scattering layer near the tropopause at high southern latitudes is not accounted for by current models, and may represent an optically thin CH_4 cloud layer condensing in a region of gentle uplift. Below this thin cloud layer, Titan’s troposphere appears clear, as these observations did not achieve the spatial resolution necessary to detect the transient CH_4 clouds recently identified near Titan’s south pole (Brown *et al.*, 2002; Roe *et al.*, 2002).

Below this complex and variable atmosphere, Titan’s surface exhibits a striking range of surface albedo at $2.0\ \mu\text{m}$, varying between 0.05 and 0.14 at a projected spatial resolution of $\sim 1200\ \text{km}$. Only one other body in the solar system exhibits similarly strong surface albedo contrast on such large spatial scales; the Earth.